Boundary Element Formulation for Partially Saturated Poroelastic Media

Peng Li[1] and Martin Schanz[2]

[1]Graz University of Technology, Institute of Applied Mechanics, Technikerstr. 4, 8010 Graz, Austria; email: tunnelee@gmail.com
[2]Graz University of Technology, Institute of Applied Mechanics, Technikerstr. 4, 8010 Graz, Austria; email: m.schanz@tugraz.at

ABSTRACT

A lot of applications, especially, in geomechanics require the computation of waves in porous media, e.g., earthquake waves in soil. Soil and other geomaterials are partial saturated poroelastic materials. Having waves in semi-infinite domains in mind a boundary element formulation for such materials seems to be preferable.

A linear theory for partial saturated poroelasticity is formulated based on the mixture theory, resulting in a set of coupled partial differential equations for the solid displacements and the pore pressures of both fluids. For such a system fundamental solutions are derived in Laplace domain with the method of Hörmander. The integral equations can be deduced based on the weighted residual technique. A standard discretisation in the spatial variable and the convolution quadrature for time discretisation yield, finally, a time stepping procedure for dynamic processes in partial saturated poroelastic media.

The validation of this method is done with the help of a 1D semi–analytical solution for a column. Finally, waves in a poroelastic half space are studied.

GOVERNING EQUATIONS

For a partially saturated porous continuum, the following assumptions are made: i) the medium is a mixture of the solid phase (index s), wetting fluid phase (index w), and non–wetting phase (index a); ii) a state transformation of the three phases is not allowed; iii) all three phases have the same temperature and any temperature change is ignored; iv) all the three phases are compressible. The governing equations are formulated following Lewis and Schrefler (1998).

With an averaging process, the porosity n and the saturation degree S_f can be defined as

$$n = \frac{V_w + V_a}{V_s + V_w + V_a} \qquad S_f = \frac{V_f}{V_s + V_w + V_a} \quad (f = w, a) \quad ,$$

where V_s, V_w and V_a represent the corresponding phase volumes. The bulk density $\rho = (1-n)\rho_s + nS_w\rho_w + nS_a\rho_a$ is the averaged density of the mixture, where ρ_s, ρ_w

and ρ_a represent the density of the solid skeleton, wetting fluid and non–wetting fluid, respectively.

The capillary pressure $p^c = p^a - p^w = p^d S_e^{-1/\vartheta}$ is based on the suggestion of Brooks and Corey (1964), where p^a and p^w are the pore air and water pressure, p^d is the non–wetting fluid entry pressure, ϑ is the pore size distribution index, and S_e denotes the effective wetting fluid saturation degree. Neglecting the osmotic suction yields the total stress

$$\sigma_{ij} = (K - \frac{2}{3}G)\delta_{ij}u_{k,k} + G(u_{i,j} + u_{j,i}) - \delta_{ij}\alpha(S_w p^w + S_a p^a) \,,$$

where G is the shear modulus and $\alpha = 1 - K/K_s$ describes the compressibility of the solid skeleton with the drained bulk modulus of the mixture K, and K_s is the bulk modulus of the solid grains. The introduction of the factor α is used to describe the compressibility of the solid grains, while $\alpha = 1$ fits to the incompressible case.

The balances of mass for the solid phase and both fluid phases are

$$\begin{aligned} \partial_t[(1-n)\rho_s] + \mathrm{div}\,[(1-n)\rho_s \partial_t u_i] &= 0 \\ \partial_t(nS_f\rho_f) + \mathrm{div}\left[nS_f\rho_f\partial_t(u_i + u_i^w)\right] &= \rho_f I^f \quad (f = w,a)\,, \end{aligned}$$

where $u_i^f (f = w,a)$ is the relative displacement of the respective fluid to the solid. $I^f (f = w,a)$ denote source terms.

The momentum balance equation for the mixture is the sum of the equations for each individual constituent, which is given by

$$Gu_{i,jj} + (K + \frac{G}{3})u_{j,ij} - \alpha(S_w p^w_{,i} + S_a p^a_{,i}) + F_i = \rho\partial_t^2 u_i + nS_w\rho_w\partial_t^2 u_i^w + nS_a\rho_a\partial_t^2 u_i^a \,, \tag{2}$$

where F_i denotes the bulk body force. The momentum balance equations for each fluid phase yield generalized Darcy's laws for each fluid phase

$$nS_f\partial_t u_i^f = -\kappa_f\left(p^f_{,i} + \rho_f\partial_t^2 u_i + \rho_f\partial_t^2 u_i^w\right) . \tag{3}$$

In (3), the coupling terms between the two fluids are neglected and the phase permeabilities ($f = w,a$) are given by $\kappa_f = \frac{K_{rf}k}{\eta_f}$. K_{rf} denotes the relative fluid phase permeability, k the intrinsic fluid permeability of a porous continuum, and η_f the viscosity of the fluid.

Equations (1), (2), and (3) are sufficient to solve the problem of partially saturated poroelasticity. The combination of the solid displacement u_i and the fluids pore pressure p^f $(f = w,a)$ is sufficient to describe the system behavior and, hence, are selected as unknowns. In time domain, however, the elimination of the relative displacement is not possible because it appears in (1), (2), and (3) in different orders of the time derivatives. Hence, the Laplace transformation is introduced to eliminate the time derivatives.

After the Laplace transformation, the relative displacements $\hat{u}_i^f$ can be substituted, and the governing equations in the Laplace domain are obtained

$$\mathscr{B}\,[\hat{u}_i,\ \hat{p}^w,\ \hat{p}^a]^\top = [-\hat{F}_i,\ -\hat{I}^w,\ -\hat{I}^a]^\top \quad ,$$

where $\mathscr{B}$ is the partial differential operator and its explicite expression can be found in Li and Schanz (2011).

FUNDAMENTAL SOLUTIONS

The fundamental solutions $\hat{U} = \hat{U}(x,y)$ of a differential operator $\mathscr{B}$ are a full space solution of the differential equations and are given by

$$\mathscr{B}^*\,\hat{U} + I\delta(x,y) = 0 \quad ,$$

where $\mathscr{B}^*$ is the adjoint operator of $\mathscr{B}$. The solution can be found following Hörmander's method. Assuming $\hat{U} = \mathscr{B}^{*co}\varphi$, where $\mathscr{B}^{*co}$ denotes the co–factors of $\mathscr{B}^*$ and φ is some scalar function. This leads to

$$\mathscr{B}^* \cdot \mathscr{B}^{*co}\varphi + I\delta(x,y) = 0 \quad \Longrightarrow \quad \det(\mathscr{B}^*)\varphi + \delta(x,y) = 0 \quad .$$

After the determination of the scalar function φ, by backward substitution, the fundamental solutions $\hat{U}$ can be determined.

The fundamental solutions have a matrix structure of nine entries, and the singular behavior of each entry can be determined by a series expansion of the exponential function. The results show that only weak singularities exist in the diagonal entries of the fundamental solutions, e.g., $\hat{U}_{ij}^{ss}$, $\hat{P}^{ww}$, and $\hat{P}^{aa}$, respectively. The other entries are all regular (Details can be found in Li (2012)).

BOUNDARY ELEMENT FORMULATION

Using in the weighted residuals method the fundamental solutions as weighting functions, the differential equations for partially saturated poroelasticity can be transformed to the integral equation. Two partial integrations with respect to the spatial variable result in the representation formula. Moving the load point $\mathbf{y}$ to the boundary, the boundary integral equations are obtained

$$\mathbf{C}(\mathbf{y})\hat{\mathbf{u}}(\mathbf{y}) = \int_\Gamma \hat{\mathbf{U}}^\top(\mathbf{y},\mathbf{x})\hat{\mathbf{t}}(\mathbf{x})d\Gamma - \oint_\Gamma \hat{\mathbf{T}}^\top(\mathbf{y},\mathbf{x})\hat{\mathbf{u}}(\mathbf{x})d\Gamma\,. \tag{4}$$

In (4), the vectors $\hat{\mathbf{u}}$ and $\hat{\mathbf{t}}$ collect the displacements and pressures and the tractions and fluxes, respectively. The tensors $\hat{\mathbf{U}}$ and $\hat{\mathbf{T}}$ denote the fundamental solutions. $\mathbf{C}(\mathbf{y})$ is the integral free term and the strong singular integral over $\hat{\mathbf{T}}$ is defined in the sense of a Cauchy Principal Value. Following the work in Messner and Schanz (2011) the

strong singular integral is analytically transformed to a weakly singular integral through integration by parts, and can be numerically solved by Duffy transformation.

To approximate the geometry, the boundary is divided into E boundary elements Γ_e via a standard triangulation. The ansatz functions $N_e^f(\mathbf{x})$ are used with the time–dependent nodal values, e.g., for the solid displacement $u_i^{ef}(t)$. The Dirichlet datum is approximated by continuous linear shape functions and the Neumann datum by discontinuous constant shape functions. By dividing the time period t in N intervals of equal duration Δt, i.e., $t = N\Delta t$, the convolution integrals between the fundamental solutions and the nodal values are approximated by the Convolution Quadrature Method (CQM, Lubich (1988)). This results in the following boundary element time stepping formulation for $n = 0, 1, 2, ..., N$

$$\sum_{e=1}^{E}\sum_{f=1}^{F}\sum_{k=0}^{n}\left\{\omega_{n-k}^{ef}(\hat{\mathbf{U}},\mathbf{y},\Delta t)^{\top}\mathbf{t}^{ef}(k\Delta t) - \omega_{n-k}^{ef}(\hat{\mathbf{T}},\mathbf{y},\Delta t)^{\top}\mathbf{u}^{ef}(k\Delta t)\right\} = \mathbf{C}(\mathbf{y})\mathbf{u}(\mathbf{y},n\Delta t)$$

with the integration weights

$$\omega_n^{ef}(\cdot,\mathbf{y},\Delta t) = \frac{\mathscr{R}^{-n}}{L}\sum_{\ell=0}^{L-1}\int_{\Gamma}\cdot\left(\mathbf{x},\mathbf{y},\frac{\gamma(\mathscr{R}e^{i\ell\frac{2\pi}{L}})}{\Delta t}\right)N_e^f(\mathbf{x})d\Gamma e^{-in\ell\frac{2\pi}{L}}\ .$$

The numerical implementation is accomplished by using the open source C++ BEM library HyENA (Messner et al., 2010).

NUMERICAL RESULTS

For all numerical examples, the surface is discretized with linear triangle elements and a BDF 2 in the CQM is used. For the material data, Massilon Sandstone as shown in table 1 is chosen. Beside, the pore size distribution index ϑ is set to 1.5, the residual water saturation S_{rw} is set to 0, and the air entry saturation S_{ra} is set to 1. The initial water saturation is set to $S_w = 0.9$.

3D Column The column has a length of 3 m, a width and height of 1 m. In order to compare with the one dimensional solution of Li and Schanz (2011), no flux at the bottom and around the column is allowed, and the normal displacement at the bottom and the four sides is also set to zero. The top of the column is excited by a stress jump according to a unit step function (Heaviside load). Furthermore, Poisson's ratio is artificially set to zero. The displacement u_z at the top center of the column, the pore water pressure p^w, and the pore air pressure p^a at the bottom center of the column are calculated. For better comparisons the dimensionless number $\beta_{CFL} = v_{p_1}\Delta t/r_e$ is introduced, where v_{p_1} is the fast compressional wave velocity and r_e is the characteristic element length. Three different surface meshes with 224 ($r_e = 1/2$ m), 896 ($r_e = 1/4$ m), and 2016 ($r_e = 1/6$ m) linear triangular elements are used to study the influence of the spatial discretization.

Table 1: Parameters of Massilon sandstone (from Murphy (1984))

Parameter type	Symbol	Value	Unit
Porosity	n	0.23	-
Density of the solid skeleton	ρ_s	2650	$\mathrm{kg/m^3}$
Density of the water	ρ_w	997	$\mathrm{kg/m^3}$
Density of the air	ρ_a	1.10	$\mathrm{kg/m^3}$
Drained bulk modulus of the mixture	K	1.02×10^9	$\mathrm{N/m^2}$
Shear modulus of the mixture	G	1.44×10^9	$\mathrm{N/m^2}$
Bulk modulus of the solid grains	K_s	3.5×10^{10}	$\mathrm{N/m^2}$
Bulk modulus of the water	K_w	2.25×10^9	$\mathrm{N/m^2}$
Bulk modulus of the air	K_a	1.10×10^5	$\mathrm{N/m^2}$
Intrinsic permeability	k	2.5×10^{-12}	$\mathrm{m^2}$
Viscosity of the water	η_w	1.0×10^{-3}	$\mathrm{Ns/m^2}$
Viscosity of the air	η_a	1.8×10^{-5}	$\mathrm{Ns/m^2}$
Gas entry pressure	p^d	5×10^4	$\mathrm{N/m^2}$

First, the influence of the spatial discretization on the results is studied. The time domain results of the displacement and pore pressure are given in figure 1 for fixed $\beta_{CFL} = 0.3$ and varying mesh size. The displacement results are nearly not influenced by the different mesh choices. Of course, the three dimensional numerical result coincides best with the 1D solution for the finest mesh with $r_e = 1/6\,\mathrm{m}$. The coarser meshes with $r_e = 1/2\,\mathrm{m}$ or $r_e = 1/4\,\mathrm{m}$ give good results, but show a somehow stronger numerical damping. However, the numerical results of all mesh sizes are acceptable.

On the other hand, the three dimensional numerical results of the pore pressure show more sensitivity with regard to the mesh size. The best results for both the pore water and pore air pressure compared with the 1D solutions are obtained if the mesh size is set to $r_e = 1/6\,\mathrm{m}$. These results can be regarded as good, whereas the results of the coarser meshes $r_e = 1/2\,\mathrm{m}$ or $r_e = 1/4\,\mathrm{m}$ deviate from the analytical solution. This trend is increased for increased time. It should be remarked that the overshooting at the wave fronts in the pressure solutions can be reduced by choosing a different multistep method within the CQM (Banjai et al., 2012). But, they can not be avoided and are not related to the partial saturated porous material.

Beside a proper mesh the time step is of much importance in dynamic calculations since it affects the result's accuracy and the efficiency. The choice of the time step should follow the rule to be small enough for the result's accuracy and as large as possible for the calculation's efficiency. The following calculations are performed with the mesh size of $r_e = 1/6\,\mathrm{m}$ but the time step size is varied by changing $\beta_{CFL} = 0.1$ to $\beta_{CFL} = 1.0$. In figure 2, the solid displacements and the pore pressures are plotted versus time for different values of β_{CFL} in comparison with the 1D solution. The displacement results (see figure 2a) are acceptable, no matter calculating with a large

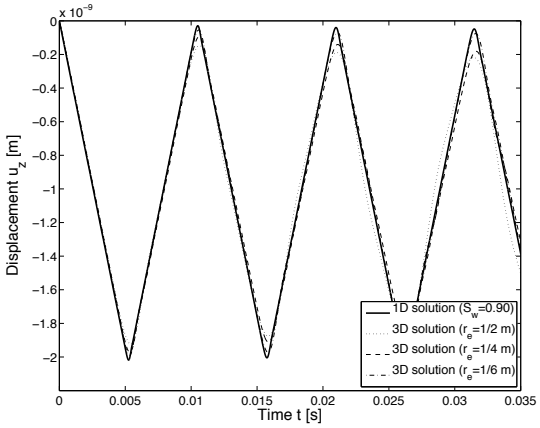

(a) Displacement u_z

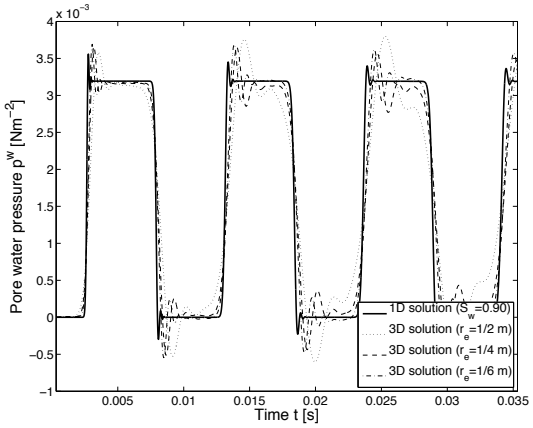

(b) Pore water pressure p^w

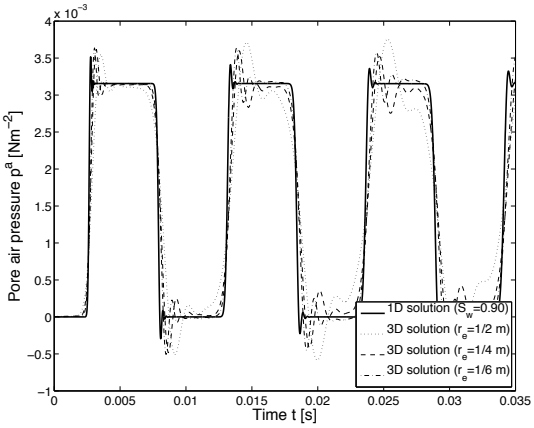

(c) Pore air pressure p^a

Figure 1: Sensitivity study on the mesh size for $\beta_{CFL} = 0.3$

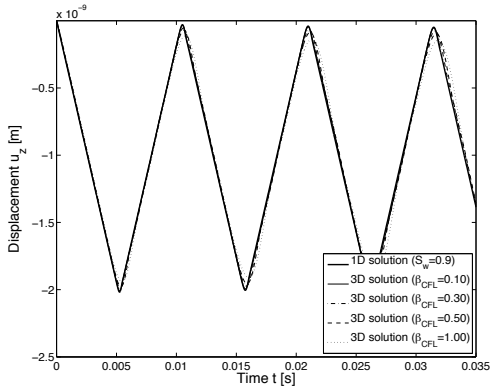

(a) Displacement u_z

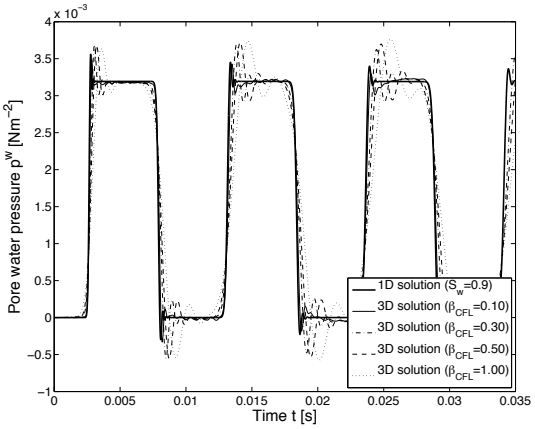

(b) Pore water pressure p^w

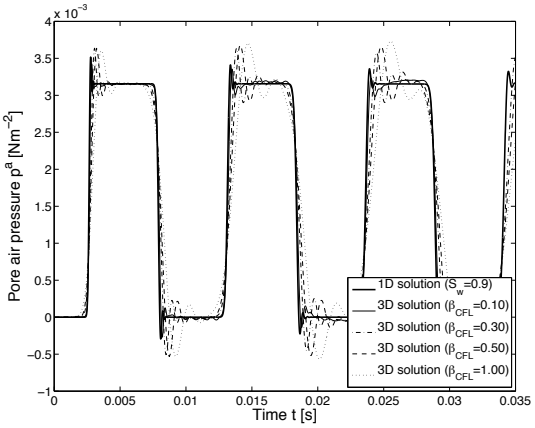

(c) Pore air pressure p^a

Figure 2: Sensitivity study on the time step size for $r_e = 1/6\,\mathrm{m}$

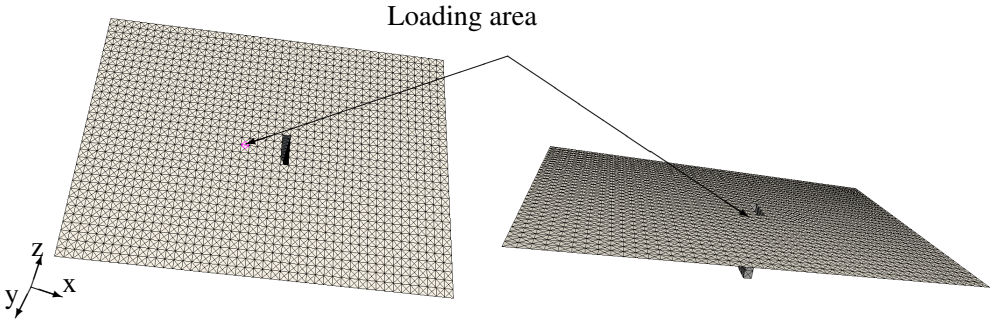

Figure 3: Surface meshes of the halspace from two perspectives

time step ($\beta_{CFL} = 1.0$, $\Delta t = 0.0001456\,\mathrm{s}$) or with a very small time step ($\beta_{CFL} = 0.1$, $\Delta t = 0.00001456\,\mathrm{s}$). The displacement results become better and better with decreasing the value of β_{CFL}, i.e., decreasing time step size. Besides, these results show no phenomenon of instability for small time step sizes as observed in other time domain BEM formulations. This may be caused by the damping of the material, i.e., the damping caused by the friction between the solid skeletton and the flowing fluid.

The pore pressure results shown in figures 2b and 2c are acceptable and nearly independent on the time step size up to $\beta_{CFL} \leq 0.5$. For a larger time step as $\beta_{CFL} = 1.0$ the result turns worse towards a larger time period, i.e., after $t = 0.015\,\mathrm{s}$.

Summarizing, the method is validated with the semi-analytical 1D solution. The displacement results are much less sensitive on the mesh size than the pore pressures. The same holds for the tractions. In comparison with an elastodynamic CQM based BEM formulation a finer mesh is required to obtain the same quality of results. This is caused by the coupling of the pore pressure with the displacements. There might be an improvement if different meshes are used for displacements and pore pressures.

Open Trench In this section, the vibration isolation of a partially saturated half space will be studied using an open trench. A square surface ($10\,\mathrm{m} \times 10\,\mathrm{m}$) is discretized with $r_e = 0.25\,\mathrm{m}$ (see figure 3). At the loading area a vertical total stress $t_z = 1\,\mathrm{Nm}^{-2} H(t)$ is applied and the remaining surface is traction free. Both, the pore water and the pore air pressure are assumed to be zero all over the surface. Three different cases are considered as case 1 (no trench), case 2 (trench depth 1 m), and case 3 (trench depth 3 m).

For a easy comparison, absolute values of the displacement amplitude $A_a = \sqrt{(u_{z_{max}} - u_{z_{min}})^2 + (u_{x_{max}} - u_{x_{min}})^2}$ are defined and calculated for each node along the center line behind the open trench. $u_{z_{max}}$ and $u_{z_{min}}$ denote the maximum and the minimum vertical displacement of the observation point, $u_{x_{max}}$ and $u_{x_{min}}$ represent the maximum and minimum radial displacement of the observation point. Since all the observation points locate in the center line of the trench according to the load, u_y is zero.

In Figure 4, the absolute values of the displacement amplitude A_a are displayed for each node along the center line behind the open trench. An amplitude reduction

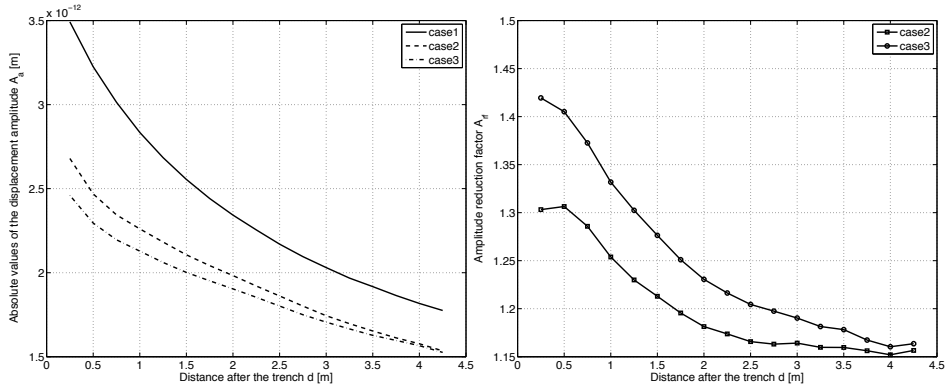

(a) Amplitude A_a (b) Reduction factor A_{rf}

Figure 4: Displacement amplitude A_a and the corresponding amplitude reduction factor A_{rf}

factor A_{rf} is also calculated by normalizing A_a to the corresponding absolute displacement without a trench. At a point 0.25 m behind the trench, the absolute value of the displacement amplitude A_a can drop from 3.5×10^{-12} m to 2.5×10^{-12} m with the deep open trench. The amplitude reduction factors of the shallow and deep open trenches are about 1.30 and 1.42, respectively. At a point 4.25 m behind the trench, the absolute value of the displacement amplitude can drop from 1.75×10^{-12} m to 1.55×10^{-12} m with the deep open trench, and the amplitude reduction factors of the shallow and deep open trenches are about 1.155 and 1.16, respectively.

In order to obtain the best effect, the position of the open trench should be as close as possible to the object to be isolated. A deeper trench will produce a better isolation effect since the traveling distance of the wave will be longer. However, taking the soil as an example, a deeper trench means a more difficult maintaining work of the trench to keep the stability as well as to avoid later back filling. A shallow trench but close enough to the object may be a viable solution, or by using an array of shallow trenches.

CONCLUSIONS

The main topic of this paper is to establish a collocation boundary element method for partially saturated poroelasticity in 3D. The material model consists of three phases, the elastic solid phase, the wetting fluid, and the non–wetting fluid. The governing equations are derived based on the principles of continuum mechanics and the mixture theory. Aiming at a Convolution Quadrature Method (CQM) based BEM it is sufficient to derive the governing equations in Laplace domain, which allows to have the solid displacements and both pore pressures as unknowns. As the singularities in the fundamental solutions are similar to the saturated case, the regularization can

be performed analogously, i.e., partial integration is used to obtain a weakly singular integral equation. After spatial discretisation and using the CQM as time discretisation a time stepping boundary element formulation for partial saturated media is obtained.

Two numerical examples are presented with the proposed boundary element formulation. First of all, the code is validated by calculating a three dimensional partially saturated poroelastic column and comparing it with an one dimensional semi-analytical solution. Two numerical parameters, the time step size and the mesh size are studied. The stability of the results is good and seems to be better as in the saturated case. An open trench is modeled in a half-space with an impulse before the trench. The displacements behind the trench at different observation points are calculated as well as the amplitude.

References

Banjai, L., Messner, M., and Schanz, M. (2012). "Runge-Kutta convolution quadrature for the boundary element method." *Comput. Methods Appl. Mech. Engrg.*, 245–246, 90–101.

Brooks, R. H. and Corey, A. T. (1964). "Hydraulic properties of porous media." *Hydraulic Papers*, Colorado State Univ.

Lewis, R. W. and Schrefler, B. A. (1998). *The Finite Element Method in the Static and Dynamic Deformation and Consolidation of Porous Media*. John Wiley and Sons, Chichester.

Li, P. (2012). *Boundary Element Method for Wave Propagation in Partially Saturated Poroelastic Contin ua*, Vol. 15 of *Computation in Engineering and Science*. Verlag der Technischen Universität Graz.

Li, P. and Schanz, M. (2011). "Wave propagation in a one dimensional partially saturated poroelastic column." *Geophys. J. Int.*, 184(3), 1341–1353.

Lubich, C. (1988). "Convolution quadrature and discretized operational calculus. I/II.." *Numer. Math.*, 52, 129–145/413–425.

Messner, M., Messner, M., Rammerstorfer, F., and Urthaler, P. (2010). "Hyperbolic and elliptic numerical analysis BEM library (HyENA). [Online; accessed 22-January-2010].

Messner, M. and Schanz, M. (2011). "A regularized collocation boundary element method for linear poroelasticity." *Comput. Mech.*, 47(6), 669–680.

Murphy, W. (1984). "Acoustic measures of partial gas saturation in tight sandstones." *J. Geophys. Res.*, 89(B13).